THE JOURNAL OF PHYSICAL CHEMISTRY C

Article

pubs.acs.org/JPCC

Exploration of the Detailed Conditions for Reductive Stability of $Mg(TFSI)_2$ in Diglyme: Implications for Multivalent Electrolytes

Artem Baskin* and David Prendergast

Molecular Foundry, Material Science Division, Lawrence Berkeley National Laboratory, Berkeley, California 94720, United States

Supporting Information

ABSTRACT: We reveal the general mechanisms of partial reduction of multivalent complex cations in conditions specific for the bulk solvent and in the vicinity of the electrified metal electrode surface and disclose the factors affecting the reductive stability of electrolytes for multivalent electrochemistry. Using a combination of *ab initio* techniques, we clarify the relation between the reductive stability of contact-ion pairs comprising a multivalent cation and a complex anion, their solvation structures, solvent dynamics, and the electrode overpotential. We found that for ion pairs with multiple configurations of the complex anion and the Mg cation whose available orbitals are partially delocalized over the molecular complex and have antibonding character, the primary factor of the reductive stability is the shape factor of the solvation sphere of the metal cation center and the degree of the convexity of a polyhedron formed by the metal cation and its coordinating atoms. We focused specifically on the details of Mg (II) bis(trifluoromethanesulfonyl)imide in diethylene glycol dimethyl ether ($Mg(TFSI)_2$)/diglyme) and its singly charged ion pair, $MgTFSI^+$. In particular, we found that both stable $(MgTFSI)^+$ and $(MgTFSI)^0$ ion pairs have the same TFSI configuration but drastically different solvation structures in the bulk solution. This implies that the MgTFSI/dyglyme reductive stability is ultimately determined by the relative time scale of the solvent dynamics and electron transfer at the Mg−anode interface. In the vicinity of the anode surface, steric factors and hindered solvent dynamics may increase the reductive stability of $(MgTFSI)^+$ ion pairs at lower overpotential by reducing the metal cation coordination, in stark contrast to the reduction at high overpotential accompanied by TFSI decomposition. By examining other solute/solvent combinations, we conclude that the electrolytes with highly coordinated Mg cation centers are more prone to reductive instability due to the chemical decomposition of the anion or solvent molecules. The obtained findings disclose critical factors for stable electrolyte design and show the role of interfacial phenomena in reduction of multivalent ions.

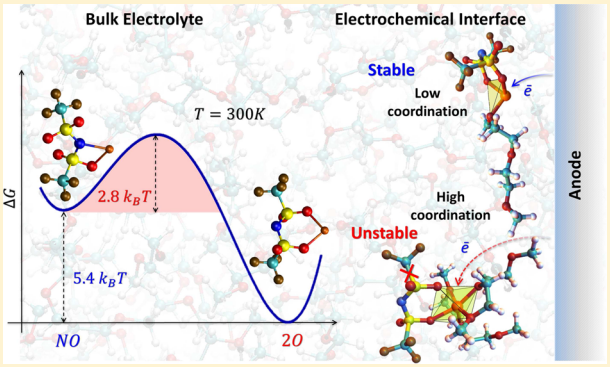

INTRODUCTION

Magnesium-based energy storage technologies attract increasing attention due to their potential to revolutionize large scale applications such as transportation and grid storage. The attractive combination of high volumetric capacity, potentially low cost, and environmentally benign character makes Mg batteries a strong candidate to provide the necessary technological advances beyond lithium ion. Promising scientific findings of Mg battery operational characteristics are potentially transformative to commercialization. Since ground-breaking innovations[1−3] in the realization of Mg-ion rechargeable batteries, significant effort has been invested in the search for an optimal combination of electrodes/electrolyte materials that would provide the desirable energy density, maximum Coulombic efficiency (CE), reversible plating/stripping of Mg, and superior cycling performance. One key parameter for Mg battery performance—the electrochemical stability of an electrolyte—has become a focus of many experimental and theoretical studies.[2−7]

The electrochemical stability of the electrolyte is largely an interfacial phenomenon whose description requires a proper handling of the absolute reference for oxidation/reduction potentials,[8−19] the accounting for the screening of charged systems,[11,12,20] and the electrode potential dependent renormalization of the quasiparticle gap of a molecule coupled to a metal surface[21−23] as well as the establishing of voltage dependence of the chemical reactions, their pathways, and transition states.[15,24,25] Accounting for the effects of solvent on the electrolyte stability constitutes another challenge for theoretical studies. By contrast with simple cations solvation evident in aqueous solutions, complex Mg-based organic salts demonstrate a significant degree of contact-ion pairing in common organic solvents even at relatively small concentrations.[26−31] The reduction of such ion pairs may involve both the Mg cation center and anion. Therefore, the solvation

Received: September 15, 2015
Revised: January 22, 2016

DOI: 10.1021/acs.jpcc.5b08999
J. Phys. Chem. C XXXX, XXX, XXX−XXX

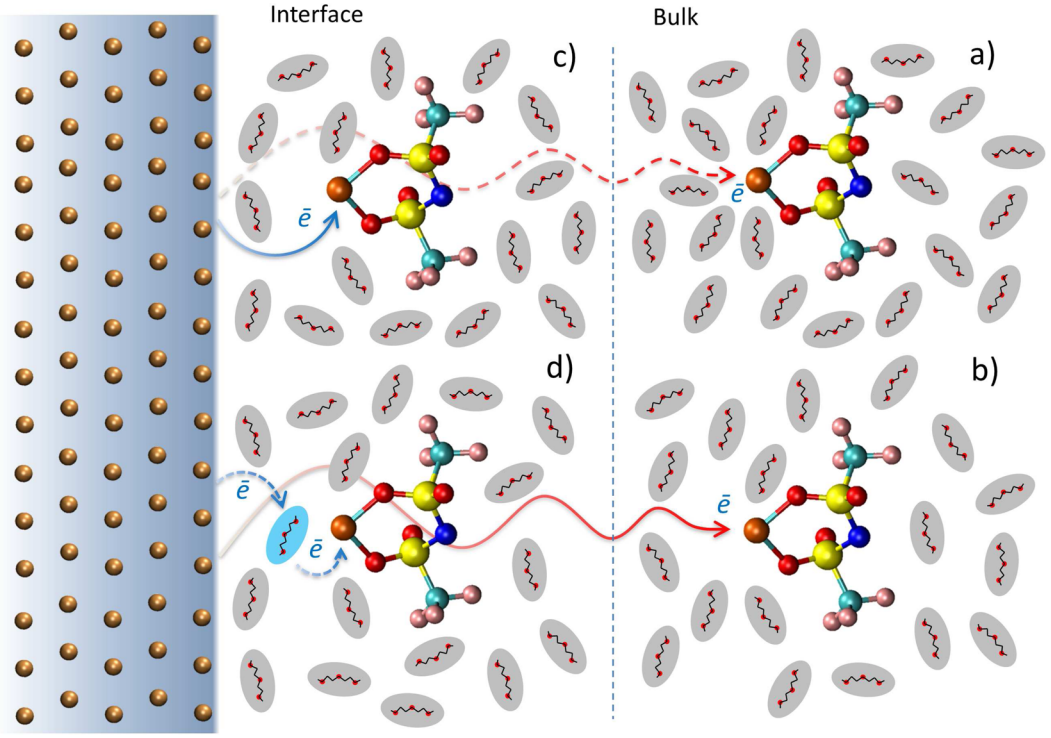

Figure 1. Schematics of possible bulk-like and interfacial mechanisms of the reduction of $(MgTFSI)^+$ ion pair solvated in diglyme. Mg atoms indicated as golden, diglyme solvent molecules encased in ellipses, and the remaining atoms constituting the $TFSI^-$ anion (C: cyan; N: blue; O: red; F: pink; S: yellow). (a) The $(MgTFSI)^+$ cation in the bulk diglyme with the Mg cation center fully coordinated by oxygens. Reduction is only possible at high overpotential (red dashed arrow). (b) Mg cation center is instantaneously undercoordinated due to solvent thermal fluctuations with resulting electron transport at lower overpotential (solid red arrow). (c) The $(MgTFSI)^+$ cation at the anode interface. The electron transfer (solid blue arrow) is facilitated by the lower Mg coordination likely induced by proximity to the surface. (d) The electron transfer mechanism via reduction of an intervening solvent molecule adsorbed on the electrode surface (dashed blue arrow).

structure of multivalent ions at each charge state is believed to critically impact the reversible plating/stripping at the anode, the ease of electrochemical deposition and related overpotential, and thus the overall CE and cycling performance.[7,32]

Since the ion configurations and their solvation structures at the interface are predetermined by those in the bulk solution, in most of the studies the electrochemical stability windows are derived from the properties of electrolytes computed for the bulk.[6,31,33,34]

However, in the conventional picture of multivalent ion deposition,[35] the details of the transition from a fully charged and highly coordinated form of a metal cation to its partially discharged and lower coordinated form remain largely unclear. The vicinity of the electrified anode surface may significantly impact the ion coordination and the solvent dynamics[36] and thus the relative time scales of the solvent reorganization and intrinsic electron transfer.[37−39] This in turn will affect the reductive stability that can be derived either from the Marcus picture of nonadiabatic electron transfer in the outer-sphere reaction governed by thermal fluctuations[40,41] or from more advanced explicit treatment of the solvent relaxation based on constrained DFT and nonadiabatic dynamics.[42−47]

Having accepted the importance of the specific spatial arrangement of coordinating solvent molecules for the reductive stability of complex ion pairs (see below the results of the current work), first we would like to provide plausible instances where that coordination might be altered in the vicinity of an electron source—the anode. In Figure 1 we outline schematically plausible mechanisms of a partial reduction of a multivalent cation (exemplified with $(MgTFSI)^+$ solvated in diglyme, see below) and highlight the difference between the reduction processes occurring in the bulk solvent and at the interface. This cartoon serves only illustrative purposes and does not claim to provide any quantitative details of the actual mechanisms. At this stage, we are guided by the general expectations of how the proximity of the electrode surface may influence the solvent dynamics and how, in its turn, it may impact the reductive stability. Below (see Discussion) we provide the theoretical rationale for the proposed mechanisms. In the bulk, the outer-sphere reaction via a nonadiabatic electron transfer can occur either at a significant overpotential to overcome the high solvent coordination of a metal cation (Figure 1a) or by assistance of solvent thermal fluctuations possibly reducing the cation coordination (Figure 1b). By contrast, at the interface, adiabatic electron transfer can be either facilitated by the reduced cation coordination assisted by the vicinity of the electrode surface and the modified solvent dynamics, e.g., adsorption of solvent molecules (Figure 1c), or mediated by the reduction of a solvent molecule sandwiched between the electrode surface and the cation (Figure 1d). This latter mechanism may or may not result from a lower Mg coordination due to the (probable) subsequent rearrangements of its solvation sphere upon solvent molecule reduction. For details see the Discussion.

Recently, electrolyte solutions based on magnesium(II) bis(trifluoromethanesulfonyl)imide $(Mg(TFSI)_2)$ in different solvents, e.g., diethylene glycol dimethyl ether (diglyme, G2) or acetonitrile (AN), were proposed as a promising candidate for advanced Mg batteries. These systems provide a relatively facile delivery of Mg^{2+} ions in a chloride-free electrolyte and an

DOI: 10.1021/acs.jpcc.5b08999
J. Phys. Chem. C XXXX, XXX, XXX−XXX

electrochemical stability (anodic limit ≥4.0 V vs Mg/Mg^{2+})[28,30,48,49] in cells with a working Mg electrode. However, these electrolytes suffer from low (≤87%) CE, significant overpotential, destructive incompatibilities with Mg metal resulting in passivation of the anode surface, and parasitic loss of electrolyte due to the electrochemical decomposition of solvent (e.g., AN) mimicking Mg-plating/insertion.[50] Another peculiarity of the $Mg(TFSI)_2$/G2 electrolyte is the debated instability of plating/stripping overpotentials at different salt concentrations and current densities.[28,50,51]

In pursuit of understanding the $Mg(TFSI)_2$ electrolyte behavior and its potential improvement, extensive computational studies were carried out.[5,6,27,31] Using a combination of classical MD simulations and quantum chemistry calculations hybridized with implicit solvent models,[52] it was shown that the solvent donor strength and its chelating ability largely determine the solubility of $Mg(TFSI)_2$ and the ion-pair solvation structure. The concentration-dependent instability of the $Mg(TFSI)_2$ salt at Mg metal potentials was assigned to a drastic decrease of dissociation energy of the C−S bond in the cation-reduced $(MgTFSI)^0$ complex leading to its decomposition into neutral $[Mg^+{-}CF_3SO_2NSO_2^-]^0$ and CF_3 fragments.[31] However, the relationship between the solute concentration and the electrochemical stability of anions is far from being fully understood and is still debated[4,6,28,30,53] since the proposed mechanism does not exclude other processes involving solvent impurities or predicted cleavage of the $(TFSI)^-$ ion on the Mg surface.[6,54]

Given the complexity and richness of the electrochemistry of the $Mg(TFSI)_2$/G2 electrolyte, we present an in-depth *ab initio* study to elucidate the connection between relevant solvation structures of complexes formed in the bulk solution and their electrochemical stability in the vicinity of the Mg metal anode and formulate a set of general guidelines for selection or design of stable electrolytes.

METHODOLOGY

The equilibrium speciation in G2 between $Mg(TFSI)_2$, Mg^{2+}, $(MgTFSI)^+$, and $(TFSI)^-$ is not yet fully studied both in bulk electrolyte and at the interface. The fundamental premise for our study of $Mg(TFSI)_2$ in diglyme is that the stability of the electrolyte is dictated by the electrochemical stability of $(MgTFSI)^+$ and its reduced form $(MgTFSI)^0$. Here, we limit our consideration solely to an elementary act (electron transfer), without any further implications for the thermally random coexistence of the fully charged and partially discharged forms of the ion pair in vicinity of each other. Moreover, we do not consider a bulk-phase coexistence of charged and neutral ion pairs either. In assumption that the proximity of the electrode surface may significantly impact the solvation structure of the $(MgTFSI)^+$ ion, we consider different fully and undercoordinated possible configurations of $(MgTFSI)^+$ in charged and partially discharged $(MgTFSI)^0$ states.

The systematic study of the correlation between the solvation structure (coordination configuration) and the mechanisms of chemical instability induced by a partial reduction in the bulk solvent is carried out in two steps. At the first step, the quantum mechanical study of small molecular clusters of $(MgTFSI)^{0/+}$ and one, two, and three G2 molecules is performed. The effects of finite temperature and condensed liquid phase on the Mg cation center coordination are accounted for by the use of *ab initio* molecular dynamics (AIMD) simulations. Since no specific assumptions about the relative time scales of the intrinsic electron transfer rate and the reorganization of the solvent at room temperature are made, we explore the structural stability (susceptibility to the decomposition upon the partial reduction) of the $(MgTFSI)^0$ unit in both relaxed and unrelaxed to the zero-charge states of the $(MgTFSI)^+$ cation solvated in G2. The accurate definition of the chemical stability of a particular configuration requires the exploration of the free energy landscape of a solute, its local minima, and transition barriers with the solvent dynamics treated explicitly. Because of the computational overheads of this approach, here we explore the local minima of the potential energy of different configurations and check their susceptibility to chemical decomposition by testing their stabilities in the condensed phase at the room temperature for at least 10 ps. We use molecular orbitals analysis as a key tool to distinguish the stable molecular configurations from unstable ones. This tool enables us an insight into the reorganization of the electron density, the hybridization of states of Mg cation, $(TFSI)^-$, and solvent diglyme molecules.

Computational Details. *Quantum Chemistry Calculations.* Optimized geometries, relative energies, and molecular orbital are calculated with the DFT TeraChem package.[55] As was reported in the previous extensive computational studies of aprotic ionic liquids,[56] traditional functionals (e.g., B3LYP) give large deviations from the high level benchmark (CCSD(T)/complete basis set) results. Insufficient basis sets (lower than 6-31 Pople family) show erroneous instability of $(MgTFSI)^0$ in the presence of any G2 molecule. However, it was found that a combination of traditional functionals with the third version of Grimme's empirical dispersion correction[57] usually produces excellent results with the 6-311++G(3df,2p) basis set.[56] In our calculations we use B3LYP-D3 functional with the 6-311++G** basis set. We use the L-BFGS geometry optimization method[58] with the termination criterion for the maximum energy gradient component of 4.5×10^{-4} au. Wave function convergence threshold is set as 3.0×10^{-5}. Two-electron integral threshold is set as 1.0×10^{-12}, and the basis set linear dependency threshold is of 1.0×10^{-4}. Partial charges were computed using the full NBO analysis. For the open shell $(MgTFSI)^0$ molecule unrestricted, KS orbitals were computed.

ESM Calculations. For the isolated and solvated in G2 $(MgTFSI)^+$ ion pair, the mutual alignment of Mg state with respect to the Mg-slab Fermi energy at different distances is evaluated within the effective screening medium (ESM) model[11,24,59] implemented in the SIESTA package.[60] This model is based on solving the Poisson's equation under open boundary conditions (or conditions dictated by the electrode environment) at $z \in (-\infty, \infty)$ separately from the Kohn−Sham equation defined for the finite cell with imposed periodic boundary conditions (PBCs). In the adiabatic limit all the electronic properties are uniquely defined by the ground state electronic density. The entire system is characterized by the common Fermi energy which accounts for the (possible) electron transfer between the slab and the molecular cluster. Thus, we do not use any specific energy level alignment scheme *a posteriori* and rely on the common E_f. The slab is modeled by a unit cell (4 × 4 × 6, 144 atoms). The distance between the exposed surface of the slab and the fictitious electrode is set as 25 Å to provide enough free space between electrodes to accommodate other species. In both cases the surface of the electrode is kept pristine and not covered by the solvent. We use the PBE functional[61] and pseudopotentials with the cutoff

DOI: 10.1021/acs.jpcc.5b08999
J. Phys. Chem. C XXXX, XXX, XXX−XXX

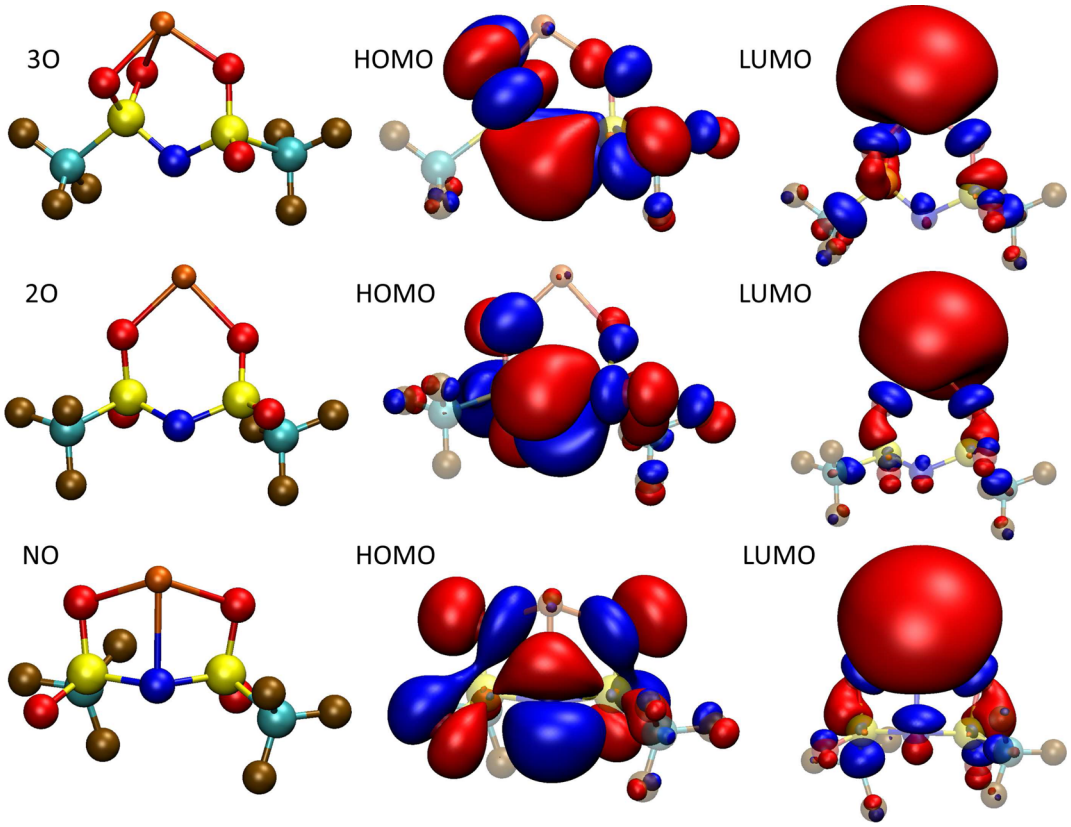

Figure 2. Most stable configurations of $(MgTFSI)^+$ where Mg is coordinated by three oxygens (3O), two oxygens (2O), and a nitrogen (NO). Corresponding HOMO and LUMO orbitals are shown. Red and blue colors of orbitals correspond to opposite phases. Mg = gold, C = cyan, S = yellow, O = red, N = blue, F = brown.

energy of 400 Ry. The non-spin-polarized static calculations are done within the eigenvalue tolerance of 10^{-4} eV, using the DZP basis. The Brillouin zones of the unit cells are sampled by the Monkhorst–Pack grid[62] with the *k*-point grid 7 × 7 × 1. Geometry optimization is carried out for all the PNCs within the conjugated gradient algorithm, until all the forces are $F <$ 0.04 eV/Å and the stress in the periodic direction is $\sigma <$ 0.01 GPa. A 6 × 6 × 4 ($a = b$ = 3.208 Å) slab with 144 Mg atoms was employed. The distance between the slab surface and the fictitious electrode was set as 25 Å. For an isolated ion pair, for each distance between Mg atom and the slab surface the position of Mg was kept fixed and the rest of the system was relaxed. For a solvated ion pair ($(MgTFSI)^+$ and six G2 molecules), for each distance between Mg atom and the slab surface, the coordinates of $(MgTFSI)^+$ were kept fixed whereas the slab and the G2 were kept free to relax.

Ab Initio Molecular Dynamics Simulations. AIMD simulations were conducted for $(MgTFSI)^{+/0}$ ion pairs in G2 at the PBE-D3 level with the TZV2PX basis set as implemented in the CP2K package.[57,63,64] As found in the previous studies,[56] this functional/basis set combination is recommended for accurate studies of energetics of ionic liquid clusters. For all AIMD simulations, the energy grid cutoff was set as 320 Ry and the total energy was sampled at the Γ-point. Using a sampling of 0.5 fs, we performed simulations of 20 ps within canonical ensemble (NVT) at 300 K with the Nosé–Hoover thermostat.[65,66] For simulations of $(MgTFSI)^+$ in G2 we used a box 23 × 23 × 23 $Å^3$ containing 23 G2 molecules and one ion pair (with an "effective" concentration of ≈0.3 M). For simulations of $(MgTFSI)^0$ in G2, a box of 22 × 22 × 22 $Å^3$ containing 19 G2 molecules (with an "effective" concentration of ≈0.37 M) was used. Preliminary 10 ns pre-equilibration NPT (P = 1 atm, T = 300 K) classical MD simulations were performed for each system to achieve the equilibrium density of G2 (0.968 g/cm^3 vs experimental value 0.937 g/cm^3) as implemented in LAMMPS[67] using GAFF/RESP force field keeping the structure of the MgTFSI unit fixed. The NBO charges of $(MgTFSI)^{+/0}$ from previous isolated clusters calculations were used. The absolute entropies of (NO) and (2O) configurations of $(MgTFSI)^+$ in G2 were computed using the two-phase thermodynamics model.[68−70]

RESULTS AND DISCUSSION

Stability of $(MgTFSI)^0$ in Diglyme: Quantum Chemistry Study of Small Molecular Clusters. Both the structure of $(MgTFSI)^0$ itself and additional diglyme molecules which coordinate Mg may affect the chemical stability of $(MgTFSI)^0$. However, the solvation structure and the molecular configuration of $(MgTFSI)^0$ are predetermined by the preferred structure of $(MgTFSI)^+$ arriving from the bulk of the solution, dynamics of intrinsic electron transfer, and solvent relaxation occurring at the Mg anode interface. We begin our study by examining the equilibrium configurations of $(MgTFSI)^+$ in the gas phase and in the G2 solvated form.

Our calculations (see Methodology) show that there are three most stable configurations of $(MgTFSI)^+$ where Mg is coordinated by (a) three oxygens (3O), (b) two oxygens (2O), and (c) nitrogen and oxygen (NO) shown in Figure 2. The corresponding bond lengths and atomic charges are summarized in Table S1. The relative formation energies and energies

DOI: 10.1021/acs.jpcc.5b08999
J. Phys. Chem. C XXXX, XXX, XXX−XXX

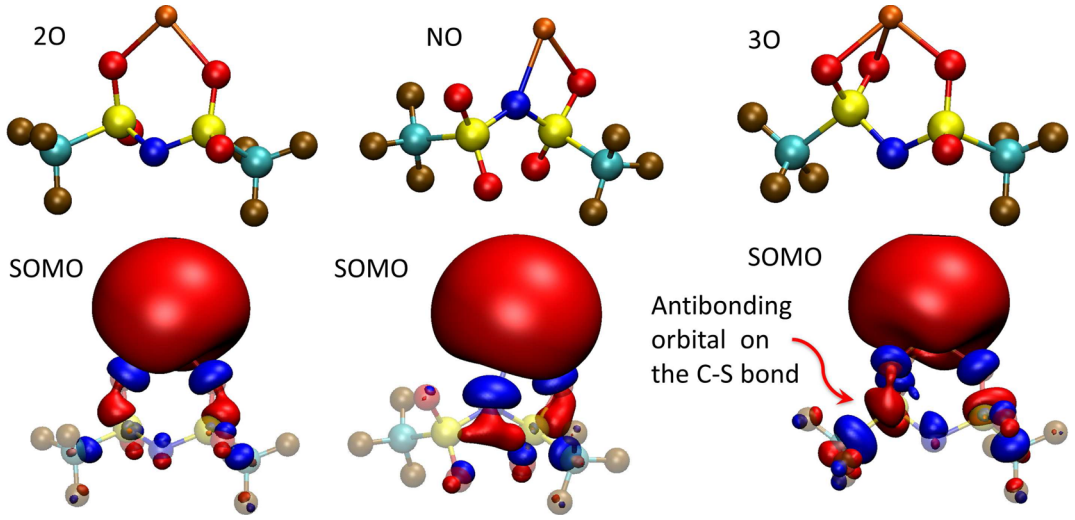

Figure 3. Most stable configurations of $(MgTFSI)^0$ where Mg is coordinated by two oxygens (2O), nitrogen (NO), and three oxygens (3O). Corresponding SOMO orbitals are shown.

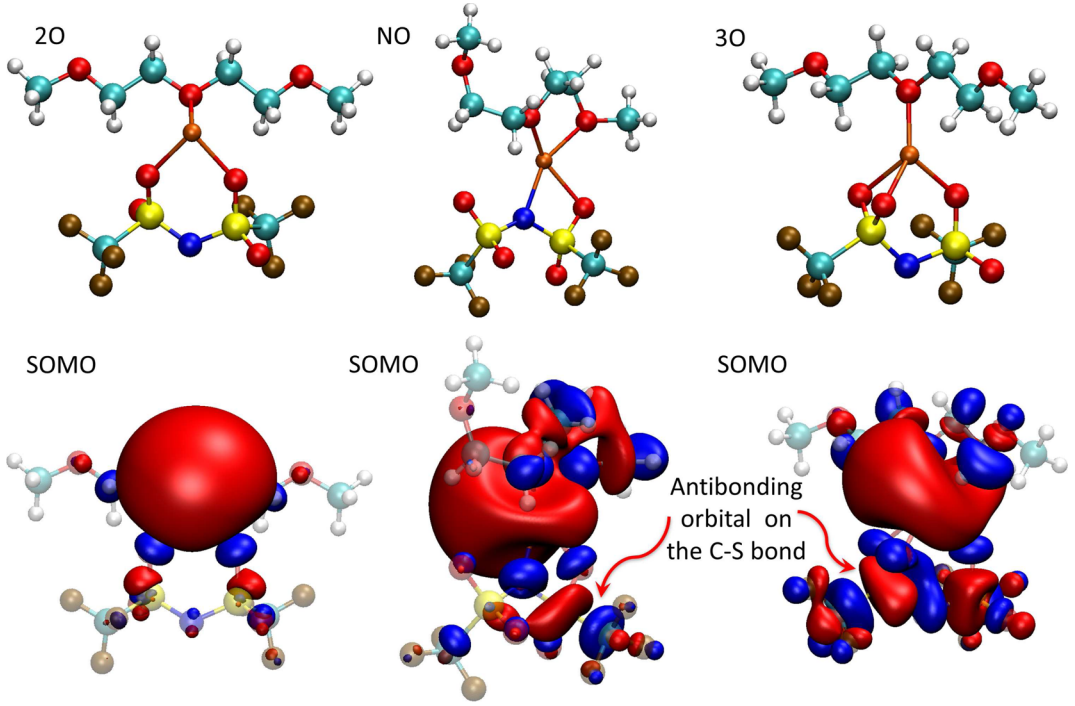

Figure 4. Configurations of $(MgTFSI)^0$ and one diglyme molecule where Mg is coordinated by two oxygens (2O), nitrogen (NO), and three oxygens (3O). The shapes of Mg coordination are trigonal pyramid, square planar, and tetrahedral, respectively. Corresponding SOMO orbitals are shown.

in parentheses corrected by accounting for vibrational enthalpies of these configurations are 0 eV, 0.038 (0.026) eV, and 0.185 (0.181) eV, respectively. Interestingly, the optimization of $Mg(TFSI)_2$ results in a structure where Mg has a tetrahedral coordination and one TFSI unit provides two oxygens whereas another TFSI unit provides nitrogen and oxygen. AIMD simulations (>10 ps) of $Mg(TFSI)_2$ show that (2O-NO) coordination dominates in the bulk G2 as well. As expected,[6,54] the electronic density is delocalized over the TFSI unit whereas the vacant orbital is largely localized on Mg, in agreement with previously reported results[31] such that an incoming electron would reside on Mg and the SOMO orbital of $(MgTFSI)^0$ would be similar to the LUMO of $(MgTFSI)^+$.

Starting from the configuration of $(MgTFSI)^+$, the geometry optimization of the partially reduced charge state $(MgTFSI)^0$ and molecular orbital analysis revealed the following results. The most stable configurations are (2O) and (NO), while the relaxation of the (3O) configuration leads to the (2O) configuration. However, we will keep all these three configurations for the analysis since they are predetermined by the fully charged form $(MgTFSI)^+$. The optimized structures are shown in Figure 3, and the corresponding bond lengths and atomic charges are summarized in Table S2. The relative formation energies and energies in parentheses corrected by accounting for vibrational enthalpies of these configurations are 0 eV, 0.332 (0.330) eV, and 0.970 (0.973) eV, respectively.

DOI: 10.1021/acs.jpcc.5b08999
J. Phys. Chem. C XXXX, XXX, XXX−XXX

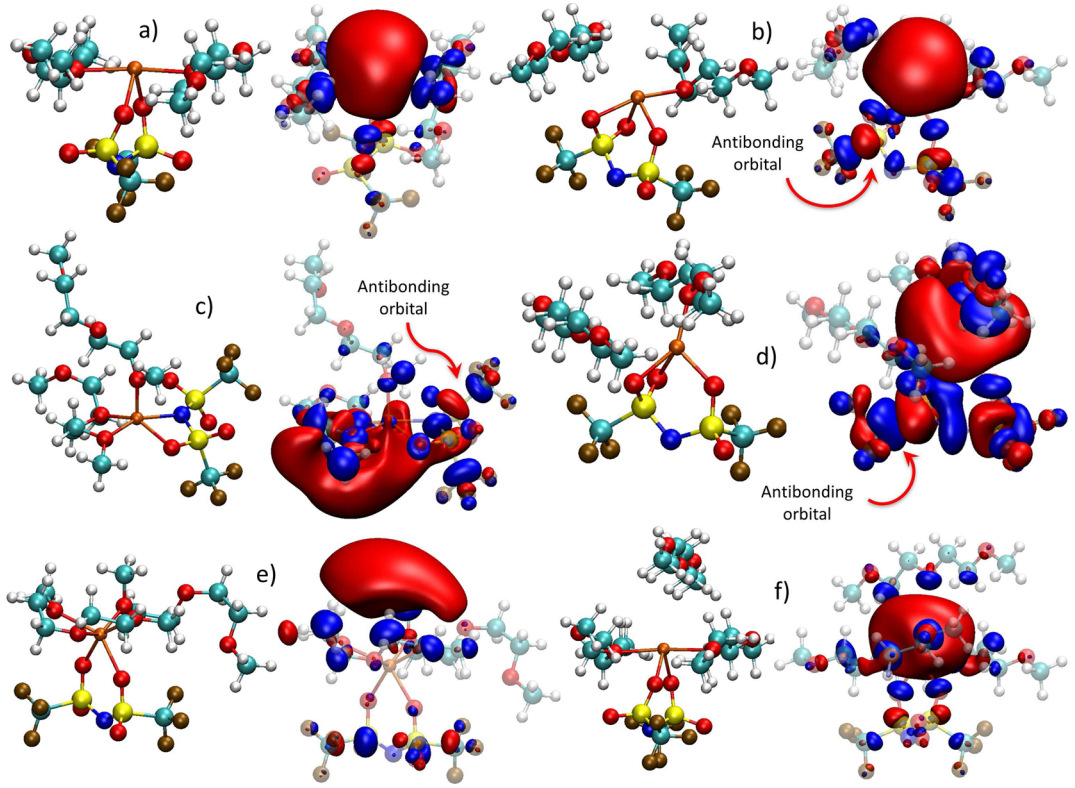

Figure 5. Configurations of $(MgTFSI)^0$ and two/three diglyme molecules with corresponding SOMO orbitals. (a) (2O) configuration; (b) (3O) configuration with two diglyme molecules preoptimized; (c) (NO) configuration; (d) (3O) configuration with nonoptimized structure of diglyme molecules; (e) (2O) configuration with two diglyme molecules chelating Mg; (f) (2O) configuration with three diglyme molecules. SOMO orbital is shown from aside.

The additional strain caused by the redundant coordination of Mg in the (3O) configuration of $(MgTFSI)^0$ and deformation of the populated Mg s-orbital lead to a slight promotion of an antibonding orbital on the C−S bond. However, it does not lead to spontaneous breaking of the C−S bond; instead the structure relaxes to the (2O) structure. At this stage, we propose an hypothesis that any possible reason for the $(MgTFSI)^0$ instability is caused by promotion of an antibonding orbital on the C−S bond caused by a significant deformation of electron density of the populated Mg s-orbital. Any geometrical constraint either from the TFSI-part or diglyme molecules resulting in deformation of the Mg s-orbital should lead to the instability of TFSI in the $(MgTFSI)^0$ complex, given that the available TFSI orbital has antibonding character at the C−S bond.

To explore this assumption, we analyze the molecular orbitals (SOMO) of $(MgTFSI)^0$ while adding gradually the diglyme molecules. The optimization of the $(MgTFSI)^0$ in the (2O) configuration and one diglyme molecule gives the structure shown in Figure 4. G2 provides only one oxygen coordinating Mg^+ and does not chelate it, in contrast with the fully solvated cation Mg^{2+}.[28,71] The overall coordinating structure is the trigonal pyramid with plenty of free space to accommodate the Mg s-orbital intact. Therefore, no pronounced antibonding orbital on the C−S bonds is observed. This is not the case for both (NO) and (3O) structures of $(MgTFSI)^0$. For a casual (NO) configuration taken from AIMD simulations of $(MgTFSI)^+$ in G2 (see below), Mg is coordinated by three oxygens and nitrogen approximately in a square-planar configuration where the nitrogen lone pair keeps Mg in the plane (see Figure 4). As one can see, a significant deformation of the Mg SOMO s-orbital leads to the promotion of an antibonding σ^* orbital on the C−S bond and its breaking. The optimization of $(MgTFSI)^+$ in (3O) configuration and one diglyme molecule results in the tetrahedral coordination of Mg with four oxygens. The optimization of $(MgTFSI)^0$ with the 4-fold Mg coordination leads to the breaking of the C−S bond due to the occupancy of the σ^* orbital. The drastic difference between 3- and 4-fold Mg coordinations reveals the role of the shape of the solvation shell and its compactness and supports our general hypothesis about the primary factor causing the instability of TFSI unit in the $(MgTFSI)^0$ complex.

Analysis of the $(MgTFSI)^0$ complex with two diglyme (see Figure 5) molecules further clarified the connection among CN, the solvation structure, and stability of the TFSI unit. Optimization of the (2O) configuration shows that Mg is 4-fold coordinated in a seesaw-shaped structure (Figure 5a) (d(O(G2)−Mg) = 2.3 Å, d(O(TFSI)−Mg) = 2.1 Å). The seesaw shape of the Mg coordination provides enough space to accommodate an electron on the Mg s-orbital without promoting an antibonding character on either C−S bond. In the case of the (3O) configuration (Figure 5 b), preoptimization of G2 molecules with fixed geometry of $(MgTFSI)^0$ also results in the seesaw shape of the Mg coordination with a slight promotion of antibonding on the C−S bond due to the redundant 3-fold coordination from the TFSI unit. However, if the initial structure of G2 enforces the tetrahedral shape of the Mg coordination (as in the $(MgTFSI)^+$ case, see Figure 5d), it promotes the significant weakening of the C−S bond and the following dissociation of the molecule. More crowded coordination of Mg, for instance, the square pyramidal (see Figure 5c), as in the case of the (NO) structure with overall 5-

DOI: 10.1021/acs.jpcc.5b08999
J. Phys. Chem. C XXXX, XXX, XXX−XXX

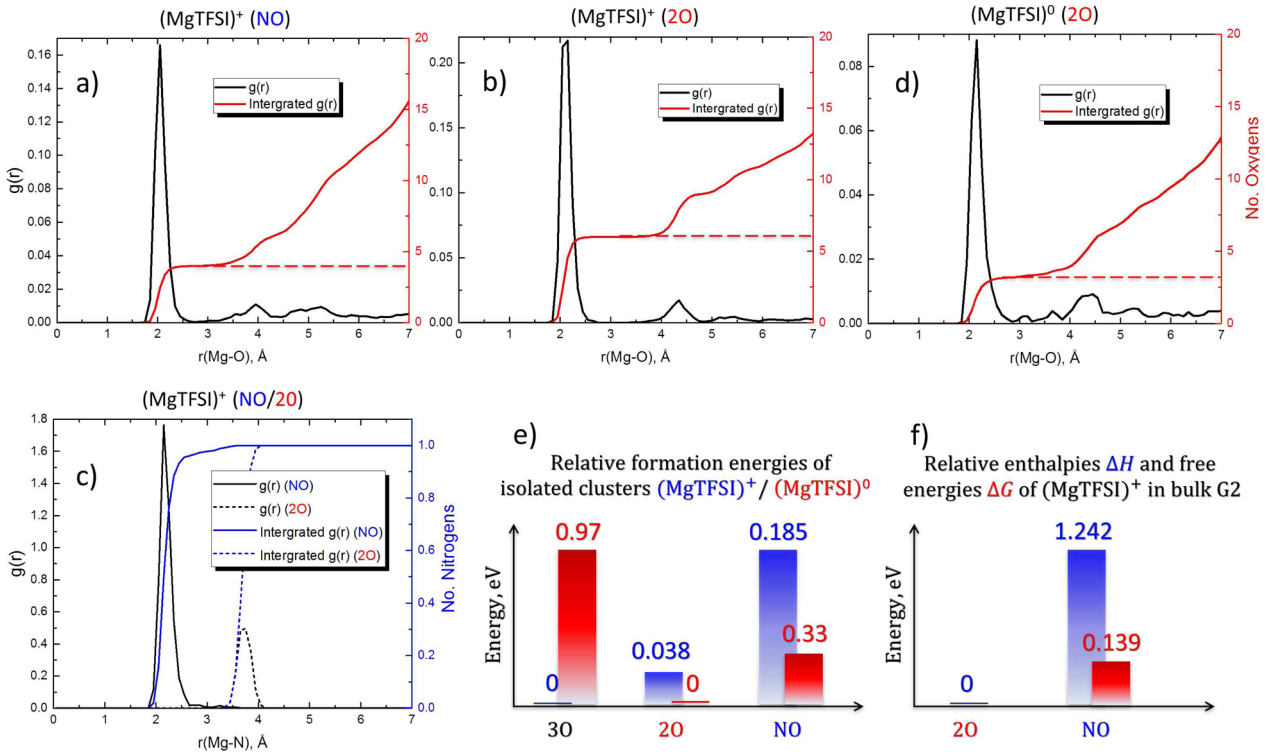

Figure 6. Pair radial distribution functions, $g(r)$, of oxygen and nitrogen in two NO and 2O configurations of $(MgTFSI)^+$ and $(MgTFSI)^0$ solvated in bulk G2. (a) $g(r)$ of oxygen in $(MgTFSI)^+$ in NO configuration, (b) $g(r)$ of oxygen in $(MgTFSI)^+$ in 2O configuration, (c) $g(r)$ of nitrogen in $(MgTFSI)^+$ in NO (solid black and blue lines) and 2O (dashed black and blue lines) configurations, (d) $g(r)$ of oxygen in $(MgTFSI)^0$ in 2O configuration, (e) relative formation energies (eV) of isolated ion pairs $(MgTFSI)^+$ (blue bars) and $(MgTFSI)^0$ (red bars) in 3O, 2O, and NO configurations. Zero energies indicate the most stable configurations; (f) relative enthalpies (eV) ΔH (blue bars) and Gibbs free energies (eV) ΔG (red bars) of $(MgTFSI)^+$ solvated in bulk G2 for 2O and NO configurations. Zero energies are for the most stable 2O configuration of $(MgTFSI)^+$ at T = 300 K.

fold coordination of Mg (taken from a snapshot of AIMD of $(MgTFSI)^+$ solvated in the bulk G2) deforms significantly the Mg s-orbital and thus promotes antibonding on the C−S bonds.

Further analysis revealed that even if Mg is chelated by two diglyme molecules and 6-fold coordinated (see Figure 5e) provided that $(MgTFSI)^0$ is in the (2O) configuration, there is still enough space to accommodate an electron on Mg s-orbital without promoting any cleavage of the TFSI unit. This observation has an important implication for the charge transfer process involving the highly coordinated Mg center of the complex cation. Highly extended LUMO orbital (Figure 5e) of $(MgTFSI)^+$ may easily hybridize with the anode surface states, thus furthering the electron transport. The optimization of (2O) structure with an additional third diglyme molecule shows that the solvated structure stabilizes in the seesaw-shaped 4-fold Mg-coordination (see Figure 5f) with no antibonding on C−S bond.

The analysis of the origin of the chemical instability would greatly benefit from the molecular level diagram reflecting the effects of the redundant Mg coordination. However, the strong coupling between the metal cation center and the TFSI unit hinders us from such an interpretation. To some extent the effects of the extra Mg coordination in the mutual alignment of the energy states as well as on their individual components can be estimated for the analysis of the PDOS of $(MgTFSI)^0$ with one diglyme molecule in (2O) and (3O) configurations (see Figure S4). As one can see, the change in coordination of Mg (an additional oxygen from TFSI) results in changes in the component contributions to the SOMO orbital: for the tetrahedral coordination, the TFSI and diglyme components become more prominent. This is compatible with the picture of the SOMO orbital (Figure 4). In addition, the change from 2O to 3O also slightly raises the energy of the frontier orbital, revealing the role of the additional coordination in stabilizing the cationic charge state of Mg. For the highly coordinated Mg (5−6 oxygens vs 3−4) this effect is expected to be more pronounced and in fact was confirmed by our ESM calculations.

The above observations allow us to draw the following conclusions. The primary factor determining the stability/instability of the TFSI unit in the $(MgTFSI)^0$/G2 complex is the shape of the Mg coordination. In order to not promote the instability, the solvation shell of Mg should be sufficiently open or ample to accommodate an extra electron on the Mg s-orbital without deforming it. A similar criterion was used[72] to explain pre-edge absorption features in the Mg K-edge spectra of Mg-MOF-74 suppressed upon specific adsorption of CO_2 at open Mg sites in that metal−organic framework due to the distortion of the local symmetry of the Mg 3s-orbital. The coordination of Mg in the first solvation sphere is highly directional due to the electron lone pairs of oxygens and nitrogen with approximately equal distances (≈2.1 Å) between Mg and other atoms coordinating it. Therefore, as a quantitative measure of the ability of the solvation sphere to accommodate an extra electron, one can use its shape factor—defined by the degree to which a polyhedron formed by Mg and coordinating atoms is convex around the Mg vertex (see Figure S1). The more the Mg polyhedron vertex protrudes outward (i.e., the smaller the

DOI: 10.1021/acs.jpcc.5b08999
J. Phys. Chem. C XXXX, XXX, XXX−XXX

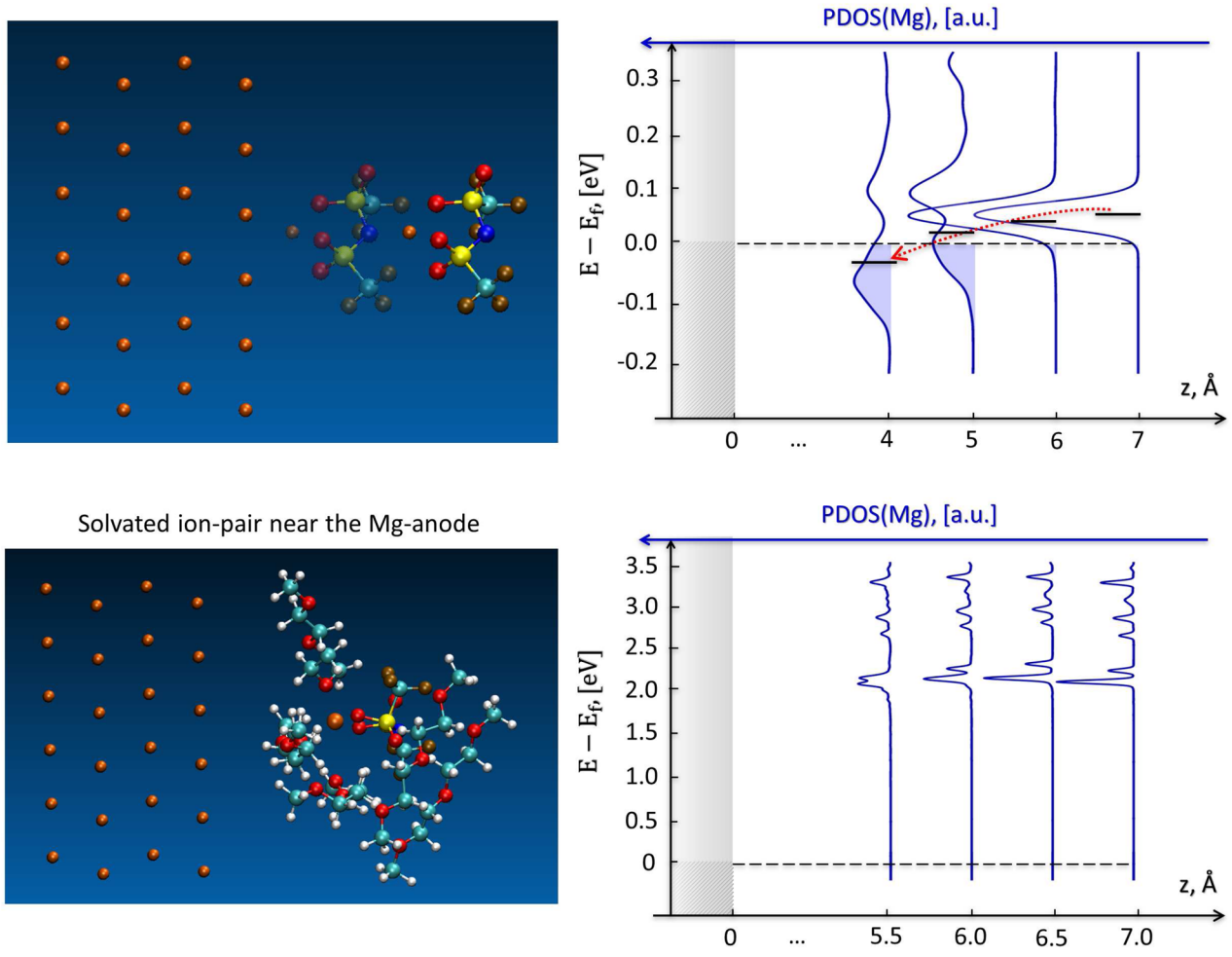

Figure 7. (top) PDOS of Mg in an isolated $(MgTFSI)^+$ ion near the Mg slab at different distances between Mg and the slab surface. (bottom) PDOS of Mg in a solvated by G2 $(MgTFSI)^+$ ion near the Mg slab at different distances.

corresponding solid angle of the polyhedron), the less the populated Mg 3s-orbital will be deformed. This criterion explains the stability of the trigonal pyramid and the seesaw configurations of $(MgTFSI)^0$ (Figure 4 (2O), Figure 5a,f) and likewise the instability of the square-planar, square-pyramid, and tetrahedral configurations (Figure 4 (NO), (3O) and Figure 5c,d).

Neither the (NO) nor (3O) structure of $(MgTFSI)^0$ can generally meet this requirement due to the steric repulsion of the electron in the Mg s-orbital by lone pairs of nitrogen or oxygens (provided by TFSI and diglyme molecules), whereas the (2O) configuration fulfills this condition. Given the fact that the (2O) configuration has the lowest energy and should dominate a thermodynamic ensemble, we conclude that the $(MgTFSI)^0$ complex in G2 is stable.

To explore other factors which can affect the stability of electrolyte, we tested two more cases: $(MgTFSI)^{0/+}$ with AN molecules and $(MgHMDS)^{0/+}$ with diglyme molecules. The electron affinity of an AN molecule is higher by ≈0.35 eV than that of a G2 molecule and can be easily hybridized with the SOMO of $(MgTFSI)^0$ (see Figure S2). Moreover, SOMO orbitals for configurations optimized for both charge states are strongly localized on the AN molecules which can explain the observed reductive instability of AN.[50] In contrast to the $(MgTFSI)^+$/G2 system, the reduction of the $(MgHMDS)^+$ pair leads to the population of an orbital localized on the solvating G2 molecules without promotion of antibonding orbitals on the HMDS anion (see Figure S3). Therefore, by this comparison, we may list additional factors which play a significant role in the selection of stable electrolytes: the relative energy alignment of LUMO orbitals of solvent molecules and ion pairs, the degree of delocalization of the LUMO orbital of the ion pair and its bonding/antibonding character, and the hybridization of LUMO orbitals of solvent molecules and the ion pair.

Solvation Structures of $(MgTFSI)^+$ and $(MgTFSI)^0$ in Bulk Diglyme: *Ab Initio* Molecular Dynamics Study. In order to further explore the reductive stability of MgTFSI-based electrolyte and account for the effects of finite temperature and condensed phase conditions, we employ AIMD to study the relevant solvation structures of $(MgTFSI)^+$ and $(MgTFSI)^0$ in G2 (for details, see Methodology). Our simulations of the $(MgTFSI)^+$ ion in G2 at room temperature exhibit two dominant configurations corresponding to (2O) and (NO) coordinations of Mg (see Figure 2) with the relative enthalpies of ≈0 and 1.24 eV, respectively, by contrast to the alignment of the formation energies of isolated $(MgTFSI)^+$ (Figure 6e,f). The estimations of the free energy barrier (NO) → (2O) give a value of $\approx 3k_BT$ at room temperature. Radial pair distribution functions of oxygens for both (2O) and (NO) configurations are shown in Figure 6a,b. The overall shape of the first coordination sphere in (2O) configuration is close to

DOI: 10.1021/acs.jpcc.5b08999
J. Phys. Chem. C XXXX, XXX, XXX−XXX

octahedral. The shape of the first coordination sphere in (NO) configuration is less symmetric. Number of oxygens coordinating Mg in these two configurations in the first solvation sphere is 4 and 6, respectively. On the other hand, these two configurations are quite distinct with respect to the nitrogen atom coordinating Mg. As seen in Figure 6c, in the (NO) configuration, nitrogen forms a short chemical bond (≈2.3 Å) with Mg whereas in the (2O) configuration the Mg−N distance is about 3.7 Å. Using the "two phase thermodynamics model" (see Methodology) we estimated the absolute entropies of (NO) and (2O) configurations. In contrast to expectations, the entropic contribution significantly reduces the enthalpy difference. The free energy difference $\Delta G_{(NO)\rightarrow(2O)}$ = 0.14 eV favoring the (2O) configuration (Figure 6f). Therefore, the equilibrium population of (NO) configuration of $(MgTFSI)^+$ ion pair versus its (2O) configuration in G2 at 300 K is ≈0.4%, suggesting that (2O) configuration is the dominant one. However, since the (NO) configuration is more entropically favored, at higher temperatures this configuration may be populated as much as the (2O) configuration. A simple estimate gives T = 338 K at which $\Delta G_{(NO)\rightarrow(2O)} = 0$ (ignoring any temperature dependence in either the enthalpy or entropy over this small range).

The AIMD simulations of $(MgTFSI)^0$ solvated in G2 show that only its (2O) (see Figure 3) configuration is stable. Mg is coordinated by ≈3 oxygens (CN = 3.2, 2 oxygens from the TFSI unit and 1 from G2 molecules; see Figure 6d). The shape of the first coordination sphere is close to trigonal pyramid with an extra oxygen aside with an ample free of atoms space around it to accommodate the 3s electron on Mg.

Discussion. The results of our quantum mechanical study of isolated clusters of $(MgTFSI)^+$ with several G2 molecules and AIMD simulations of the ion pair in the bulk G2 solvent show that the most dominant configuration of the $(MgTFSI)^+$ ion is the (2O) configuration where Mg is coordinated by 6 oxygens. On the other hand, we found that the $(MgTFSI)^0$ complex in the (2O) configuration is the only stable configuration whereas others (NO and 3O) are not and decompose by the C−S break. However, the coordination of Mg in $(MgTFSI)^0$ in the bulk G2 is significantly lower (CN = 3.2), and any higher coordination promotes instability on the TFSI unit. Therefore, the ultimate reductive stability of MgTFSI/G2-based electrolyte is determined by dynamics of the solvent and the electron transfer at the Mg−anode interface.

Since the equilibrium configuration of the MgTFSI ion pair in the charged and discharged states is the same (2O), the overall process of the reduction can be viewed as an outer-sphere reaction. If the electron transfer is much faster than the reorganization of the solvent, then upon reduction the $(MgTFSI)^0$ will decompose due to the compactness of its solvation sphere as schematically shown in Figure 1a. However, this is only possible at the relatively high overpotential. Alternatively, the resonant electron transition at the lower overpotential may be assisted by solvent thermal fluctuations reducing the CN of the metal cation. In this case displayed in Figure 1b $(MgTFSI)^0$ will remain stable after the charge reduction of $(MgTFSI)^+$. The probability of such an event is believed to be small due to the large free energy barrier associated with a spontaneous drastic change of the CN. On the other hand, the vicinity of the electrified electrode surface may switch the electron transfer mechanism and modify the solvent dynamics and thus the reductive stability of the electrolyte.

To clarify the role of the interface, we use the ESM model (see Methodology) to perform the analysis of the Mg PDOS for the isolated and solvated in G2 $(MgTFSI)^+$ ion near the Mg surface. The results are shown in Figure 7. Because of its high electron affinity and a significant coupling to the Mg surface states even at 5−6 Å (Figure 7, top panel), the bare $(MgTFSI)^+$ ion easily reduces via adiabatic electron transfer. On the other hand, the dipolar field generated by solvating G2 molecules stabilizes the Mg cation, preventing the electron transfer by shifting Mg 3s level well above the E_f (Figure 7, bottom panel). Therefore, at small anode overpotentials, highly coordinated $(MgTFSI)^+$ ions remain unreduced and thus stable. As one can see from Figure S5, the solvent empty states are well above the Fermi energy and are not expected to get involed into the reduction. The change of the DOS of the slab states (when molecular cluster is at 5.5 Å distance) is caused by its interactions with diglyme molecules.

However, the coordination of Mg in $(MgTFSI)^+$ at the interface may get reduced due to the hindered dynamics of G2 molecules adsorbed on the anode surface providing less oxygens for the Mg cation and/or due to thermal fluctuations of the solvent in the double layer (Figure 1c). Therefore, the surface layer solvent molecules may prevent to some extent the electron transfer but at the same time reduce the risk of the reductive instability of $(MgTFSI)^0$. Assuming the limitations of both the ESM model and our computations setup for the interface, one should keep in mind that the discussion of the reductive stability if the cation in terms of the surface overpotential and the cation solvation energy cannot be well performed here since we miss the thermodynamic component. The electrode potential was not set at the equilibrium of the reaction $Mg^{2+} + 2e \Leftrightarrow Mg^0$. Therefore, the conversion of the cation LUMO screening energy by the solvent molecules into the units for the overpotential remains largely unclear, as is the quantitative discussion of the surface assisted hindrance of the solvent dynamics influencing the solvation structure of the cation-pair. That would require a fully self-consistent computational procedure with an explicit treatment of the electron transfer reaction. In this case, the LUMO screening potential (∼2 V; see Figure 7, bottom panel) could serve as a first rough estimate of the overpotential at which the electron transfer reaction would go efficiently.

Another mechanism remaining heretofore unexplored implies the $(MgTFSI)^+$ reduction mediated by the reduction of the adsorbed solvent molecule (Figure 1d). Because of the high local electric field induced by the anode and the cation, the G2 solvent molecule sandwiched in between may accept and then pass the electron to the Mg cation center. For such an electron-rich molecule as a diglyme molecule, the reduction does not however lead to its fragmentation as we checked by our quantum mechanical calculations of an isolated diglyme molecule and in conditions when it is in between the Mg surface and the $(MgTFSI)^+$ ion (using the constrained DFT). Therefore, this scenario does not refer to the solvent decomposition. Upon possible structural rearrangements (e.g., repulsion of other solvent molecules) following or parallel to the G2 molecule reduction, the Mg coordination may be reduced, thus facilitating the electron transfer from the G2 molecule to the ion pair and favoring its reductive stability.

CONCLUSION

Using a combination of quantum chemistry calculations with AIMD simulations, in this work we explored the factors

DOI: 10.1021/acs.jpcc.5b08999
J. Phys. Chem. C XXXX, XXX, XXX−XXX

determining the reductive stability of electrolytes for multivalent ions, specifically, the $Mg(TFSI)_2$/diglyme system. We found that for ion pairs with multiple points of contact between the Mg cation and this complex anion both the internal ion-pair configuration and the solvation structure of the Mg cation center are important factors in determining bulk reductive stability. Moreover, the entropic contribution to the overall solvation free energy of different ion-pair configurations is an important factor as much as their enthalpies. In particular, in the condensed phase, there are two major configurations of $(MgTFSI)^+$ where Mg is coordinated either by two oxygens or by one nitrogen and one oxygen from TFSI, whose relative population at room temperature is 1:0.004 (albeit with a significant temperature dependence driven by entropy). In the fully solvated (2O) coordination of the $(MgTFSI)^+$ cation, Mg is coordinated on average with 5−6 oxygens, whereas in the stable (2O) configuration of the reduced $(MgTFSI)^0$ ion pair in bulk diglyme, Mg is coordinated by only 3−4 oxygens. The primary factor in the $(MgTFSI)^+$/diglyme reductive stability is the shape factor of its solvation sphere (defined by the convexity of the polyhedron formed by Mg and its coordinating atoms and by the steric angle of the polyhedron at the Mg vertex) that determines the ease of the accommodation of an electron in the Mg 3s-orbital. We also considered the role of the interface in lowering the risk of reductive instability of $(MgTFSI)^0$. By examining other solvent combinations ($(MgTFSI)^+$/AN, $(MgHMDS)^+$/diglyme), we found that the degree of delocalization of the LUMO orbital of the ion pair, its antibonding character, and the relative alignment of LUMO orbitals of solute and solvent and degree of their hybridization are the key factors to consider when selecting a stable electrolyte. All results we obtained suggest that for an electrolyte with a high coordination of the multivalent metal cation the risk of reductive instability generally increases.

■ ASSOCIATED CONTENT

Supporting Information

The Supporting Information is available free of charge on the ACS Publications website at DOI: 10.1021/acs.jpcc.5b08999.

Summary table of equilibrium geometries and atomic charges for different configurations of $(MgTFSI)^+$, summary table of equilibrium geometries and atomic charges for different configurations of $(MgTFSI)^0$, schematics of solvation shape factors for the Mg cation, the optimized geometries and SOMO orbitals for $(MgTFSI)^{+/0}$ with one or two AN molecules, the optimized geometries and SOMO orbitals for $(MgHMDS)^{+/0}$ with one AN molecule, PDOS of $(NgTFSI)^0$ with the diglyme molecule for (2O) and (3O) configurations, PDOS of the solvent (diglyme) and Mg slab in a solvated $(MgTFSI)^+$ ion near the Mg slab at different distances between Mg and the slab surface (PDF)

■ AUTHOR INFORMATION

Corresponding Author

*E-mail abaskin@lbl.gov; Ph +1 510 4866123; Fax +1 510 4867424 (A.B.).

Notes

The authors declare no competing financial interest.

■ ACKNOWLEDGMENTS

This work was supported by the Joint Center for Energy Storage Research, an Energy Innovation Hub funded by the U.S. Department of Energy, Office of Science, Basic Energy Sciences. Portions of this work were supported by a User Project at The Molecular Foundry and its compute cluster (vulcan), managed by the High Performance Computing Services Group, at Lawrence Berkeley National Laboratory (LBNL), and portions of this work used the computing resources of the National Energy Research Scientific Computing Center, LBNL, both of which are supported by the Office of Science of the U.S. Department of Energy under Contract DE-AC02-05CH11231. Authors thank Pieremanuele Canepa, Kevin R. Zavadil, and Tod Pascal for useful comments on the manuscript.

■ REFERENCES

(1) Aurbach, D.; Lu, Z.; Schechter, A.; Gofer, Y.; Gizbar, H.; Turgeman, R.; Cohen, Y.; Moshkovich, M.; Levi, E. Prototype Systems for Rechargeable Magnesium Batteries. *Nature* **2000**, *407*, 724−727.

(2) Yoo, H. D.; Shterenberg, I.; Gofer, Y.; Gershinsky, G.; Pour, N.; Aurbach, D. Mg Rechargeable Batteries: an On-Going Challenge. *Energy Environ. Sci.* **2013**, *6*, 2265−2279.

(3) Muldoon, J.; Bucur, C. B.; Oliver, A. G.; Sugimoto, T.; Matsui, M.; Kim, H. S.; Allred, G. D.; Zajicek, J.; Kotani, Y. Electrolyte Roadblocks to a Magnesium Rechargeable Battery. *Energy Environ. Sci.* **2012**, *5*, 5941−5950.

(4) Benmayza, A.; Ramanathan, M.; Arthur, T. S.; Matsui, M.; Mizuno, F.; Guo, J.; Glans, P.-A.; Prakash, J. Effect of Electrolytic Properties of a Magnesium Organohaloaluminate Electrolyte on Magnesium Deposition. *J. Phys. Chem. C* **2013**, *117*, 26881−26888.

(5) Cheng, L.; Assary, R. S.; Qu, X.; Jain, A.; Ong, S. P.; Rajput, N. N.; Persson, K.; Curtiss, L. A. Accelerating Electrolyte Discovery for Energy Storage with High-Throughput Screening. *J. Phys. Chem. Lett.* **2015**, *6*, 283−291.

(6) Kim, D. Y.; Lim, Y.; Roy, B.; Ryu, Y.-G.; Lee, S.-S. Operating Mechanisms of Electrolytes in Magnesium Ion Batteries: Chemical Equilibrium, Magnesium Deposition, and Electrolyte Oxidation. *Phys. Chem. Chem. Phys.* **2014**, *16*, 25789−25798.

(7) Pour, N.; Gofer, Y.; Major, D. T.; Aurbach, D. Structural Analysis of Electrolyte Solutions for Rechargeable Mg Batteries by Stereoscopic Means and DFT Calculations. *J. Am. Chem. Soc.* **2011**, *133*, 6270−6278.

(8) Nielsen, M.; Björketun, M. E.; Hansen, M. H.; Rossmeisl, J. Towards First Principles Modeling of Electrochemical Electrode-Electrolyte Interfaces. *Surf. Sci.* **2015**, *631*, 2−7.

(9) Rossmeisl, J.; Skúlason, E.; Björketun, M. E.; Tripkovic, V.; Norskov, J. K. Modeling the Electrified Solid - Liquid Interface. *Chem. Phys. Lett.* **2008**, *466*, 68−71.

(10) Björketun, M. E.; Zeng, Z.; Ahmed, R.; Tripkovic, V.; Thygesen, K. S.; Rossmeisl, J. Avoiding Pitfalls in the Modeling of Electrochemical Interfaces. *Chem. Phys. Lett.* **2013**, *555*, 145−148.

(11) Otani, M.; Sugino, O. First-principles Calculations of Charged Surfaces and Interfaces: A Plane-Wave Nonrepeated Slab Approach. *Phys. Rev. B: Condens. Matter Mater. Phys.* **2006**, *73*, 115407.

(12) Letchworth-Weaver, K.; Arias, T. A. Joint Density Functional Theory of the Electrode-Electrolyte Interface: Application to Fixed Electrode Potentials, Interfacial Capacitances, and Potentials of Zero Charge. *Phys. Rev. B: Condens. Matter Mater. Phys.* **2012**, *86*, 075140.

(13) Reed, S. K.; Lanning, O. J.; Madden, P. A. Electrochemical Interface Between an Ionic Liquid and a Model Metallic Electrode. *J. Chem. Phys.* **2007**, *126*, 084704.

(14) Rungger, I.; Chen, X.; Schwingenschlögl, U.; Sanvito, S. Finite-bias Electronic Transport of Molecules in a Water Solution. *Phys. Rev. B: Condens. Matter Mater. Phys.* **2010**, *81*, 235407.

(15) Tripkovic, V.; Björketun, M. E.; Skúlason, E.; Rossmeisl, J. Standard Hydrogen Electrode and Potential of Zero Charge in Density

DOI: 10.1021/acs.jpcc.5b08999
J. Phys. Chem. C XXXX, XXX, XXX−XXX

Functional Calculations. *Phys. Rev. B: Condens. Matter Mater. Phys.* **2011**, *84*, 115452.
(16) Cheng, J.; Sprik, M. Alignment of Electronic Energy Levels at Electrochemical Interfaces. *Phys. Chem. Chem. Phys.* **2012**, *14*, 11245−11267.
(17) Pham, T. A.; Lee, D.; Schwegler, E.; Galli, G. Interfacial Effects on the Band Edges of Functionalized Si Surfaces in Liquid Water. *J. Am. Chem. Soc.* **2014**, *136*, 17071−17077.
(18) Kharche, N.; Muckerman, J. T.; Hybertsen, M. S. First-Principles Approach to Calculating Energy Level Alignment at Aqueous Semiconductor Interfaces. *Phys. Rev. Lett.* **2014**, *113*, 176802.
(19) Leung, K. Predicting the Voltage Dependence of Interfacial Electrochemical Processes at Lithium-Intercalated Graphite Edge Planes. *Phys. Chem. Chem. Phys.* **2015**, *17*, 1637−1643.
(20) Jinnouchi, R.; Anderson, A. B. Electronic Structure Calculations of Liquid-Solid Interfaces: Combination of Density Functional Theory and Modified Poisson-Boltzmann Theory. *Phys. Rev. B: Condens. Matter Mater. Phys.* **2008**, *77*, 245417.
(21) Neaton, J. B.; Hybertsen, M. S.; Louie, S. G. Renormalization of Molecular Electronic Levels at Metal-Molecule Interfaces. *Phys. Rev. Lett.* **2006**, *97*, 216405.
(22) Sau, J. D.; Neaton, J. B.; Choi, H. J.; Louie, S. G.; Cohen, M. L. Electronic Energy Levels of Weakly Coupled Nanostructures: C_{60}-Metal Interfaces. *Phys. Rev. Lett.* **2008**, *101*, 026804.
(23) Souza, A. M.; Rungger, I.; Pemmaraju, C. D.; Schwingenschloegl, U.; Sanvito, S. Constrained-DFT Method for Accurate Energy-Level Alignment of Metal/Molecule Interfaces. *Phys. Rev. B: Condens. Matter Mater. Phys.* **2013**, *88*, 165112.
(24) Bonnet, N.; Morishita, T.; Sugino, O.; Otani, M. First-Principles Molecular Dynamics at a Constant Electrode Potential. *Phys. Rev. Lett.* **2012**, *109*, 266101.
(25) Bonnet, N.; Dabo, I.; Marzari, N. Chemisorbed Molecules under Potential Bias: Detailed Insights from First-Principles Vibrational Spectroscopies. *Electrochim. Acta* **2014**, *121*, 210−214.
(26) Mohtadi, R.; Matsui, M.; Arthur, T. S.; Hwang, S.-J. Magnesium Borohydride: From Hydrogen Storage to Magnesium Battery. *Angew. Chem., Int. Ed.* **2012**, *51*, 9780−9783.
(27) Lapidus, S. H.; Rajput, N. N.; Qu, X.; Chapman, K. W.; Persson, K. A.; Chupas, P. J. Solvation Structure and Energetics of Electrolytes for Multivalent Energy Storage. *Phys. Chem. Chem. Phys.* **2014**, *16*, 21941−21945.
(28) Ha, S.-Y.; Lee, Y.-W.; Woo, S. W.; Koo, B.; Kim, J.-S.; Cho, J.; Lee, K. T.; Choi, N.-S. Magnesium(II) Bis(trifluoromethane sulfonyl) Imide-Based Electrolytes with Wide Electrochemical Windows for Rechargeable Magnesium Batteries. *ACS Appl. Mater. Interfaces* **2014**, *6*, 4063−4073.
(29) Tutusaus, O.; Mohtadi, R. Paving the Way towards Highly Stable and Practical Electrolytes for Rechargeable Magnesium Batteries. *ChemElectroChem.* **2015**, *2*, 51−57.
(30) Shao, Y.; Rajput, N. N.; Hu, J.; Hu, M.; Liu, T.; Wei, Z.; Gu, M.; Deng, X.; Xu, S.; Han, K. S.; Wang, J.; Nie, Z.; et al. Nanocomposite Polymer Electrolyte for Rechargeable Magnesium Batteries. *Nano Energy* **2015**, *12*, 750−759.
(31) Rajput, N. N.; Qu, X.; Sa, N.; Burrell, A. K.; Persson, K. A. The Coupling between Stability and Ion Pair Formation in Magnesium Electrolytes from First-Principles Quantum Mechanics and Classical Molecular Dynamics. *J. Am. Chem. Soc.* **2015**, *137*, 3411−3420.
(32) Xu, K.; von Wald Cresce, A. Li^+-Solvation/Desolvation Dictates Interphasial Processes on Graphitic Anode in Li Ion Cells. *J. Mater. Res.* **2012**, *27*, 2327−2341.
(33) Ong, S. P.; Andreussi, O.; Wu, Y.; Marzari, N.; Ceder, G. Electrochemical Windows of Room-Temperature Ionic Liquids from Molecular Dynamics and Density Functional Theory Calculations. *Chem. Mater.* **2011**, *23*, 2979−2986.
(34) Goodenough, J. B.; Kim, Y. Challenges for Rechargeable Li Batteries. *Chem. Mater.* **2010**, *22*, 587−603.
(35) Pinto, L. M. C.; Quaino, P.; Santos, E.; Schmickler, W. On the Electrochemical Deposition and Dissolution of Divalent Metal Ions. *ChemPhysChem* **2014**, *15*, 132−138.
(36) Canepa, P.; Gautam, G. S.; Malik, R.; Jayaraman, S.; Rong, Z.; Zavadil, K. R.; Persson, K.; Ceder, G. Understanding the Initial Stages of Reversible Mg Deposition and Stripping in Inorganic Nonaqueous Electrolytes. *Chem. Mater.* **2015**, *27*, 3317−3325.
(37) Vakarin, E. V.; Holovko, M. F.; Piotrowiak, P. Ion-pairing Effects in Intramolecular Electron Transfer. *Chem. Phys. Lett.* **2002**, *363*, 7−12.
(38) Marichev, V. Experimental Approach to the Anion Problem in DFT Calculation of the Partial Charge Transfer During Adsorption at Electrochemical Interfaces. *Chem. Phys. Lett.* **2005**, *411*, 434−438.
(39) Marichev, V. Partial Charge Transfer During Anion Adsorption: Methodological Aspects. *Surf. Sci. Rep.* **2005**, *56*, 277−324.
(40) Calef, D. F.; Wolynes, P. G. Classical Solvent Dynamics and Electron Transfer. 1. Continuum Theory. *J. Phys. Chem.* **1983**, *87*, 3387−3400.
(41) Gosavi, S.; Marcus, R. A. Nonadiabatic Electron Transfer at Metal Surfaces. *J. Phys. Chem. B* **2000**, *104*, 2067−2072.
(42) Wu, Q.; Van Voorhis, T. Direct Calculation of Electron Transfer Parameters through Constrained Density Functional Theory. *J. Phys. Chem. A* **2006**, *110*, 9212−9218.
(43) Wu, Q.; Van Voorhis, T. Extracting Electron Transfer Coupling Elements from Constrained Density Functional Theory. *J. Chem. Phys.* **2006**, *125*, 164105.
(44) Wu, Q.; Van Voorhis, T. Constrained Density Functional Theory and Its Application in Long-Range Electron Transfer. *J. Chem. Theory Comput.* **2006**, *2*, 765−774.
(45) Akimov, A. V.; Prezhdo, O. V. The PYXAID Program for Non-Adiabatic Molecular Dynamics in Condensed Matter Systems. *J. Chem. Theory Comput.* **2013**, *9*, 4959−4972.
(46) Akimov, A. V.; Neukirch, A. J.; Prezhdo, O. V. Theoretical Insights into Photoinduced Charge Transfer and Catalysis at Oxide Interfaces. *Chem. Rev.* **2013**, *113*, 4496−4565.
(47) Akimov, A. V.; Prezhdo, O. V. Nonadiabatic Dynamics of Charge Transfer and Singlet Fission at the Pentacene/C60 Interface. *J. Am. Chem. Soc.* **2014**, *136*, 1599−1608.
(48) Arthur, T. S.; Singh, N.; Matsui, M. Electrodeposited Bi, Sb and Bi1-xSbx Alloys as Anodes for Mg-ion Batteries. *Electrochem. Commun.* **2012**, *16*, 103−106.
(49) Shao, Y.; Gu, M.; Li, X.; Nie, Z.; Zuo, P.; Li, G.; Liu, T.; Xiao, J.; Cheng, Y.; Wang, C.; Zhang, J.-G.; Liu, J. Highly Reversible Mg Insertion in Nanostructured Bi for Mg Ion Batteries. *Nano Lett.* **2014**, *14*, 255−260.
(50) Tran, T. T.; Lamanna, W. M.; Obrovac, M. N. Evaluation of Mg[N(SO2CF3)2]2/Acetonitrile Electrolyte for Use in Mg-Ion Cells. *J. Electrochem. Soc.* **2012**, *159*, A2005−A2009.
(51) Lossius, L. P.; Emmenegger, F. Plating of Magnesium from Organic Solvents. *Electrochim. Acta* **1996**, *41*, 445−447.
(52) Kelly, C. P.; Cramer, C. J.; Truhlar, D. G. Aqueous Solvation Free Energies of Ions and Ion-Water Clusters Based on an Accurate Value for the Absolute Aqueous Solvation Free Energy of the Proton. *J. Phys. Chem. B* **2006**, *110*, 16066−16081.
(53) Wan, L. F.; Prendergast, D. The Solvation Structure of Mg Ions in Dichloro Complex Solutions from First-Principles Molecular Dynamics and Simulated X-ray Absorption Spectra. *J. Am. Chem. Soc.* **2014**, *136*, 14456−14464.
(54) Kim, H.; Muldoon, J.; Matsu, M. High Energy Density Mg Battery Systems, 217th ECS Meeting, Abstract 225, 2012.
(55) Ufimtsev, I. S.; Martinez, T. J. Quantum Chemistry on Graphical Processing Units. 3. Analytical Energy Gradients, Geometry Optimization, and First Principles Molecular Dynamics. *J. Chem. Theory Comput.* **2009**, *5*, 2619−2628.
(56) Zahn, S.; MacFarlane, D. R.; Izgorodina, E. I. Assessment of Kohn-Sham Density Functional Theory and Moeller-Plesset Perturbation Theory for Ionic Liquids. *Phys. Chem. Chem. Phys.* **2013**, *15*, 13664−13675.
(57) Grimme, S.; Antony, J.; Ehrlich, S.; Krieg, H. A Consistent and Accurate Ab Initio Parametrization of Density Functional Dispersion Correction (DFT-D) for the 94 Elements H-Pu. *J. Chem. Phys.* **2010**, *132*, 154104.

DOI: 10.1021/acs.jpcc.5b08999
J. Phys. Chem. C XXXX, XXX, XXX−XXX

(58) Kästner, J.; Carr, J. M.; Keal, T. W.; Thiel, W.; Wander, A.; Sherwood, P. DL-FIND: An Open-Source Geometry Optimizer for Atomistic Simulations†. *J. Phys. Chem. A* **2009**, *113*, 11856−11865.
(59) Hamada, I.; Sugino, O.; Bonnet, N.; Otani, M. Improved Modeling of Electrified Interfaces Using the Effective Screening Medium Method. *Phys. Rev. B: Condens. Matter Mater. Phys.* **2013**, *88*, 155427.
(60) Sánchez-Portal, D.; Ordejón, P.; Artacho, E.; Soler, J. M. Density-Functional Method for Very Large Systems with LCAO Basis Sets. *Int. J. Quantum Chem.* **1997**, *65*, 453−461.
(61) Perdew, J. P.; Zunger, A. Self-Interaction Correction to Density-Functional Approximations for Many-Electron Systems. *Phys. Rev. B: Condens. Matter Mater. Phys.* **1981**, *23*, 5048−5079.
(62) Monkhorst, H. J.; Pack, J. D. Special Points for Brillouin-Zone Integrations. *Phys. Rev. B* **1976**, *13*, 5188−5192.
(63) VandeVondele, J.; Hutter, J. Gaussian Basis Sets for Accurate Calculations on Molecular Systems in Gas and Condensed Phases. *J. Chem. Phys.* **2007**, *127*, 114105.
(64) Hutter, J.; Iannuzzi, M.; Schiffmann, F.; VandeVondele, J. CP2K: Atomistic Simulations of Condensed Matter Systems. *Wiley Interdiscip. Rev.: Comput. Mol. Sci.* **2014**, *4*, 15−25.
(65) Nosé, S. A. Unified Formulation of the Constant Temperature Molecular Dynamics Methods. *J. Chem. Phys.* **1984**, *81*, 511−519.
(66) Hoover, W. G. Canonical Dynamics: Equilibrium Phase-Space Distributions. *Phys. Rev. A: At., Mol., Opt. Phys.* **1985**, *31*, 1695−1697.
(67) Plimpton, S. Fast Parallel Algorithms for Short-Range Molecular Dynamics. *J. Comput. Phys.* **1995**, *117*, 1−19.
(68) Lin, S.-T.; Blanco, M.; Goddard, W. A. The Two-Phase Model for Calculating Thermodynamic Properties of Liquids from Molecular Dynamics: Validation for the Phase Diagram of Lennard-Jones Fluids. *J. Chem. Phys.* **2003**, *119*, 11792−11805.
(69) Lin, S.-T.; Maiti, P. K.; Goddard, W. A. Two-Phase Thermodynamic Model for Efficient and Accurate Absolute Entropy of Water from Molecular Dynamics Simulations. *J. Phys. Chem. B* **2010**, *114*, 8191−8198.
(70) Pascal, T. A.; Lin, S.-T.; Goddard, W. A., III Thermodynamics of Liquids: Standard Molar Entropies and Heat Capacities of Common Solvents from 2PT Molecular Dynamics. *Phys. Chem. Chem. Phys.* **2011**, *13*, 169−181.
(71) Sutjianto, A.; Curtiss, L. A. Li^+-Diglyme Complexes: Barriers to Lithium Cation Migration. *J. Phys. Chem. A* **1998**, *102*, 968−974.
(72) Drisdell, W. S.; Poloni, R.; McDonald, T. M.; Long, J. R.; Smit, B.; Neaton, J. B.; Prendergast, D.; Kortright, J. B. Probing Adsorption Interactions in Metal-Organic Frameworks using X-ray Spectroscopy. *J. Am. Chem. Soc.* **2013**, *135*, 18183−18190.

DOI: 10.1021/acs.jpcc.5b08999
J. Phys. Chem. C XXXX, XXX, XXX−XXX